




Improving adhesive behavior of fiber reinforced composites by incorporating electrospun Polyamide-6,6 nanofibers in joining region

Journal of Composite Materials
2022, Vol. 56(29) 4449–4459
© The Author(s) 2022
Article reuse guidelines:
sagepub.com/journals-permissions
DOI: 10.1177/00219983221133478
journals.sagepub.com/home/jcm


Gözde Esenoğlu¹, Murat Barisik¹ , Metin Tanoğlu¹ , Melisa Yeke¹, Ceren Türkdoğan¹, Hande İplikçi¹, Seçkin Martin¹, Kaan Nuhoglu¹, Engin Aktaş² , Serkan Dehneliler³ and Mehmet Erdem İriş³

Abstract

Adhesive joining of fiber reinforced polymer (CFRP) composite components is demanded in various industrial applications. However, the joining locations frequently suffer from adhesive bond failure between adhesive and adherent. The aim of the present study is improving bonding behavior of adhesive joints by electrospun nanofiber coatings on the prepreg surfaces that have been used for composite manufacturing. Secondary bonding of woven and unidirectional CFRP parts was selected since this configuration is preferred commonly in aerospace practices. The optimum nanofiber coating with a low average fiber diameter and areal weight density is succeeded by studying various solution concentrations and spinning durations of the polyamide-6.6 (PA 66) electrospinning. We obtained homogeneous and beadless nanofiber productions. As a result, an average diameter of 36.50 ± 12 nm electrospun nanofibers were obtained and coated onto the prepreg surfaces. Prepreg systems with/without PA 66 nanofibers were hot pressed to fabricate the CFRP composite laminates. The single-lap shear test coupons were prepared from the fabricated laminates to examine the effects of PA 66 nanofibers on the mechanical properties of the joint region of the composites. The single-lap shear test results showed that the bonding strength is improved by about 40% with minimal adhesive use due to the presence of the electrospun nanofibers within the joint region. The optical and SEM images of fractured surfaces showed that nanofiber-coated joints exhibited a coherent failure while the bare surfaces underwent adhesive failure. The PA66 nanofibers created better coupling between the adhesive and the composite surface by increasing the surface area and roughness. As a result, electrospun nanofibers turned adhesive failure into cohesive and enhanced the adhesion performance composite joints substantially.

Keywords

carbon fiber-reinforced polymers, adhesive bonding, electrospinning and electrospun nanofibers, polyamide-6,6, lap-shear test

Introduction

The popularity of composite materials in the aviation industry is constantly increasing.¹⁻³ Most of the high-performance structural composites used in aviation applications include layers of prepreps which provide many advantages such as high corrosion resistance, high strength, low weight, and better fatigue strength.⁴ However, the joints are the weakest part of the manufactured structures.⁵ The traditional mechanical fasteners, screws, and rivets have adverse effects such as increasing weight, creating stress concentrations, deteriorating the structural capacity of the components, affecting electromagnetic properties/radar absorption

properties, etc. Instead, adhesive bonding appears as an advantageous alternative, and the search for successful

¹Department of Mechanical Engineering, Izmir Institute of Technology, Turkey

²Department of Civil Engineering, Izmir Institute of Technology, Turkey

³TUSAŞ (Turkish Aerospace Industries Inc), Turkey

Corresponding author:

Metin Tanoğlu, Department of Mechanical Engineering, Izmir Institute of Technology, Iztech Gulbahce Campus, Mech. Eng. Building, Urla, İzmir 35430, Turkey.

Email: metintanoglu@iyte.edu.tr

bonding methodologies became a critical engineering challenge.

There are three basic methods of adhesive joining of composite parts for manufacturing composite structures.⁶ First, joining can be done simultaneously with curing both parts, called co-curing. Since both parts are in wet condition, co-curing can be performed with or without the inclusion of an adhesive. The second method is co-bonding, where one material was cured before joining the process to an uncured or partially cured part with an adhesive at the interface. The third option is secondary bonding, where two cured parts are joined using some adhesives. Commonly, co-curing and co-bonding are preferred to reduce the curing cycles. However, this might not be technically feasible depending on the size of the parts and/or manufacturing orders. For example, connecting small composite spars into large composite wings requires secondary bonding techniques.^{7,8} Specifically, small parts are often produced using woven (twill) prepreg fabrics, while large ones are produced preferably with unidirectional (UD) prepregs. Therefore, secondary bonding of woven and UD composite parts is common in many aerospace applications.

The success of joining processes is frequently assessed by the lap shear test in literature. Multiple researchers report that the highest joint strength performance is obtained using co-curing or secondary bonding.⁵ Especially joining complex structures, secondary bonding outperforms the other two methods.⁹⁻¹¹ Researchers further looked into failure mechanisms at the joint interfaces. The most common problem was an adhesive failure which developed due to interfacial bond failure between the adhesive and the adherent.^{11,12} Researchers observed that increasing the adhesive thickness enhanced the adhering of adhesive to the surface.^{5,13} However, this results in undesired weight gain. Secondary bonding appeared as the best option to join small parts onto large ones. However, alternative methodologies for enhanced interfacial coupling between adhesive and composite surface are still under investigation.

In recent years, the incorporation of nanofibers produced by electrospinning into the matrix phase has been utilized to enhance material properties.¹⁴⁻¹⁸ It is an active research topic to incorporate nanofibers as an interface agent in the composite material production from prepregs to increase material strength. Electrospinning proved an effective method for producing continuous nanofibers with easy control of fiber diameter and functionality by adjusting polymer solution composition and voltage.^{19,20} Recent studies presented the use of thermoplastic nanofibers for improving composite strength without sacrificing in-plane mechanical properties. The interspersed low-weight thermoplastic nanofiber covers were found to increase the interlayer Mode I, Mode II, and interlayer fracture toughness of carbon fiber/epoxy laminates.^{21,22} Most of the studies in the literature have focused on electrospinning of the

polyamide-6.6 (PA 66) nanofibers due to their superior properties such as high mechanical strength, high processability, exceptional fiber-forming ability, high melting temperature, high compatibility with uncured resin, low heat deflection temperature, and low moisture absorption capacity.^{14,23-25} In addition, nanofibers produced by electrospinning can be produced by adding various filler materials such as CNT, graphene, nano-diamond. A number of study reported in the literature indicated that the structures can be strengthened by adding filler materials.²⁶⁻²⁹ However, it is one of the difficulties to ensure the homogeneous distribution of these fillers in the resin. The inclusion of micro or nanofillers in the resin liquid adversely affects the homogeneity and viscosity of the resin. The influence of nanofiber coating on the surface wetting behavior was also considered in literature. The PA66 nanofibers are found highly absorbent.³⁰ Studies reported enhanced wetting by PA66 nanofiber coating observed as substantial decrease in contact angle.^{31,32} However, the literature search conducted on the use of electrospun nanofibers for secondary bonding joints is very limited.

In this study, electrospun PA 66 nanofibers on the joining interface of carbon fiber-reinforced polymer (CFRP) composite parts for a secondary bonding process are studied for the first time in literature. Since it is common in many aerospace applications, joining UD and woven prepreg composite parts is studied herein. An optimization process on application parameters is run by checking different solution ratios of PA 66 with varying thicknesses on the joining interfaces. The morphology (homogeneity and bead-free structure) of the created nanofiber layer is examined by Scanning Electron Microscope (SEM). At the same time, the thermal properties are tested by Differential Scanning Calorimetry (DSC) analysis. The mechanical performance of the joints was assessed by lap-shear tests, and the joint locations after failure had been examined. The effect of electrospinning of PA66 nanofibers on the joint performance is quantified by the change in shear strength capacity of the joint.

Experimental

Materials

Unidirectional (UD) carbon fiber prepreg fabrics with the unit weight of 350 g/m² and woven carbon fiber prepreg fabrics with the unit weight of 475 g/m² are used. Film adhesive (FM300KTM) was used as an adhesive. PA66 pellets (Sigma Aldrich-429171) were utilized in the electrospinning process. Formic acid (Sigma Aldrich-27001) and chloroform (Sigma Aldrich-24216) were used as solvents for PA66 pellets, similar to the literature.³³

Table 1.

Table 1. Pre- and post-cure thicknesses of UD and Woven prepregs, FM300 K (1 layer) film adhesive and PA66 nanofibers (10 %wt-3 min and 10 min).

	Average thickness (mm)	
	Pre-curing	Post-curing
UD Prepreg	0.156	0.142
Woven Prepreg	0.310	0.290
FM300 K (1 layer)	0.200	0.160
PA66 nanofibers (10%wt-3min)	0.006	0.006
PA66 nanofibers (10%wt-10min)	0.021	0.020

The ply thickness of the UD and woven prepregs after curing are 0.142 mm and 0.290 respectively, and the average thickness of the adhesive FM300 K is 0.16 mm. Negligible change in the thickness of the PA66 nanofibers after curing validates the unharmed nanofiber system.

Preparation of PA 66 solutions for electrospinning

The solution parameters were studied to determine optimum parameters for a homogeneous nanofiber formation. Before solution preparations, PA66 pellets were heated and kept at 80° for 24 h to remove moisture. Different solution ratios were prepared by dissolving 10%, 12%, 14%, and 18% weight ratio of PA 66 pellets in 100 mL of formic acid/chloroform (75:25 v/v) at room temperature. The presence of chloroform in the PA66/formic-acid solution increased the viscosity of the solution, which supported to produce of more homogeneous nanofibers. This concentration was chosen based on the findings reported in our previous study.^{14,33}

Deposition of PA 66 nanofibers on carbon prepregs

PA 66 nanofibers were produced with the electrospinning setup shown in Figure 1. The Innovento PE 300TM electrospinning device, which is very suitable for automation, was used. The system was tested for homogeneity (z-axis movement) and different coating properties, and also for scaling the production parameters such as changing the horizontal movement between 10-80 mm and 5-50 mm/sec and the nozzle number between 1 and 18 with the collector spinning at a distance between 30-230 mm automatically. The setup has a nanofibr membrane production capacity adjustable between 0.01 and 5 gr/m² so that the weight gain was controlled precisely.

The prepared PA66 polymer liquid was filled into two 50 mL syringes connected to the propellant pump. The optimum parameters to produce uniform and bead-free PA 66 nanofibers were determined based on our experience and following the literature recommendations.²⁴ The flow rate

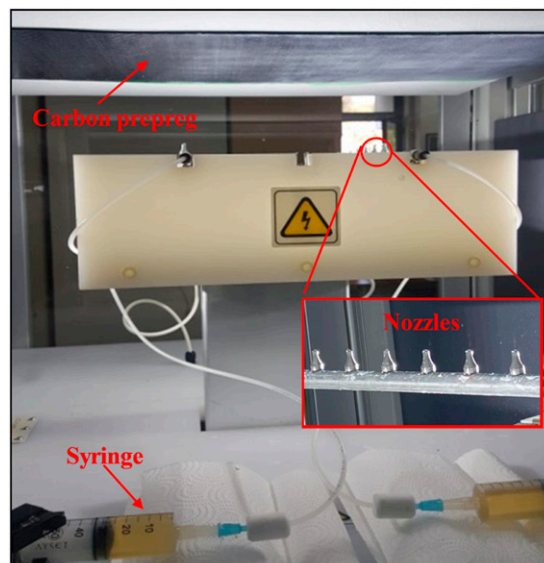


Figure 1. The electro-spinning and continuous substrate winding collector system with 0.01–5 gr/m² production capacity and ease of automation.

of the PA 66 solution was determined to be 18 mL/hr (1.0 mL/hr for each nozzle). The applied voltage and nozzle/fiber distance were optimized as 30 kV and 12 cm, respectively. Using these parameters, nanofibers were successfully applied onto the prepreg surface continuously. To examine the effects of Area Weight Density (AWD) of nanofibers coated over the prepregs, the spinning duration (3, 7, and 10 min) was varied. Figure 2(a) presents the winding prepreg during operation. Closer views of the prepreg surface at two different spinning durations of 3 min and 10 min are given in Figure 2(b). Nanofiber deposition can be seen with the naked eye as a color change after electrospinning (Figure 2(b)). Figure 2(c) presents the SEM image of 10 min electrospun surfaced as an example with the size of the nanofibers. First, the morphology of the produced nanofibers shows a continuous and uniform nanofiber network without bead formation. The nanofiber diameter distribution was between 35.99 nm and 54.63 nm, while the average diameter was 36.52 ± 12 nm. Most of the previous studies report an average PA66 nanofiber diameter in the range of 80–300 nm. To keep the weight gain minimum, average fiber diameters and AWD values lower than the reported in the literature^{14,22,33,34} When the SEM images and test results in this study are examined, it is clear that an increase in the mechanical performance is achieved at a minimal weight increase by reducing the nanofiber diameter.

Contact angle measurements were carried out in our laboratory using the KSV AttensionTM Theta device. Wetting angles were measured on each surface at three different locations. Variation of contact angle on bare and

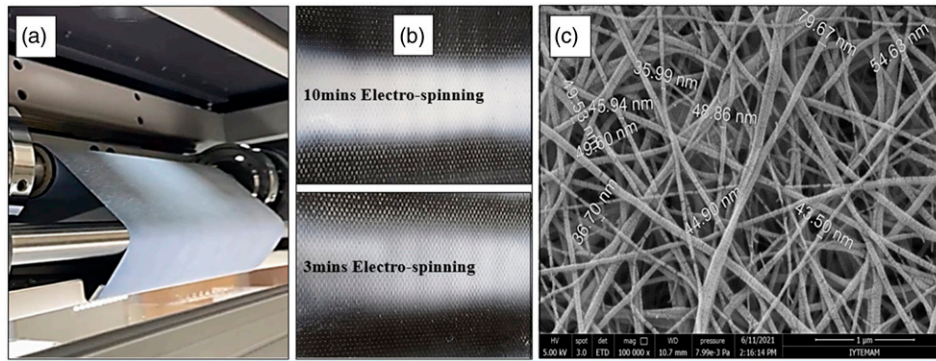


Figure 2. a) The image of the nanofiber-coated prepreps in the collector, b) The image of the 3 and 10 min coated samples, and c) SEM images of 10 wt% PA 66 nanofibers at 100,000X magnification.

PA66 nanofiber coated surfaces are given in Figure 3. Water droplet remains in a spherical bead form on bare prepreg surface after a slight contact angle decrease due to the limited water absorption of composite system. A contact angle close to hydrophobic behavior is observed on uncoated prepreg surface ($\sim 80^\circ$). On the other hand, very strong water absorption developed when the surface is coated by PA66 nanofibers. Similar to literature, PA66 showed high water absorption.³⁰ In order to resolve the behavior better, we measured wetting angles through a very short time interval. In a few seconds, contact angle converged to zero value on PA66 nanofiber coated surfaces. We observed that increasing the coating thickness decreased the time required for complete water absorption.

Differential scanning calorimetry (DSC) was used to determine the thermal properties of the electrospun PA 66 veils. The spin sample taken from the surface of four different carbon prepreg fabrics were heated from room temperature to 350°C at a heating rate of $10^\circ\text{C}/\text{min}$ under a nitrogen atmosphere. Figure 4 shows the DSC curve of the PA 66 nanofibers. The melting temperature (T_m) and the glass transition temperature (T_g) of PA66 nanofibers were 262.25°C and 48.83°C , respectively.

Manufacturing of composite laminates

Twelve-layer unidirectional prepreg CFRP fabrics at [45/0/45/90/-45/0]s order and eight-layer woven prepreg CFRP fabrics at [45/0/45/0]s with and without electrospun PA66 nanofiber coating were produced using the hot press method as shown in Figure 5.

Prepreps were prepared based on the fabrication procedure described in Figure 6. Prepreps were left to cure for 2 h under 5 bar pressure in a hot press device set at 180°C beforehand and laminated. The surfaces of the laminates bonded were prepared by cleaning with acetone prior to bonding procedure. The joint samples prepared by placing two and three layers of film adhesive (FM300 K) between

two composite prepreg parts and they were left to cure for 2 h under 3 bar pressure in a hot press device adjusted to 180°C .

Adhesive joining of the UD and woven CFRP parts

UD and woven parts were bonded together using the FM300 K as our adhesive material. The film adhesive (FM300 K) used in our work is in a form of high viscosity film. Since it is not in a liquid form as paste adhesives, air bubble formation wasn't observed. Moreover, the film adhesive used is an aerospace grade material which is commonly used in commercial applications that does not tolerate defect formations such as bubbles. Figure 7 illustrates the process where both interfaces at the joining area was coated by electrospun PA66 nanofibers. In order to investigate the effect of adhesive thickness, different specimens were produced with two and three layers of adhesives creating 0.4 mm and 0.6 mm of adhesive thicknesses, respectively.

Next, specimens were produced for the lap shear test according to the ASTM D5868 standards, as shown in Figure 8 (b). UD and woven parts were joined with and without PA66 nanofiber coating at their interface. The manufactured composite samples were cut in desired dimensions with a water-cooled diamond saw. The cut edges of the samples were lightly sanded by hand with 280 grit sandpaper.

Single-lap shear test

Mechanical testing of adhesively joint UD and woven CFRPs using single-lap shear test were performed. The setup of the lap joint is given in Figure 8(a). MTS Landmark™ Servo-hydraulic Test System was used. The load was applied at a constant crosshead speed of 13 mm/min until the fracture, according to ASTM standard D5868-01. At least five samples were tested for each type of the

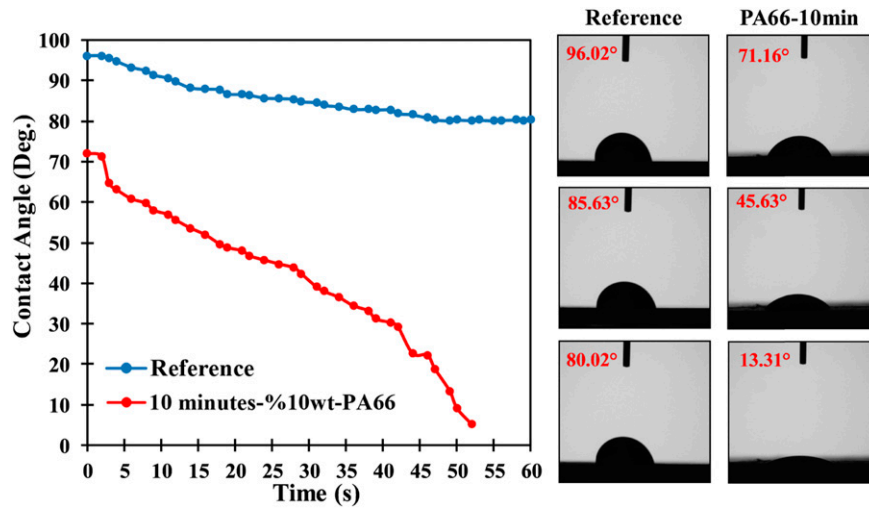


Figure 3. The wetting angle variation and droplet images of uncoated prepreg surface (reference) and 10 min 10% wt-PA66 coated surface by time.

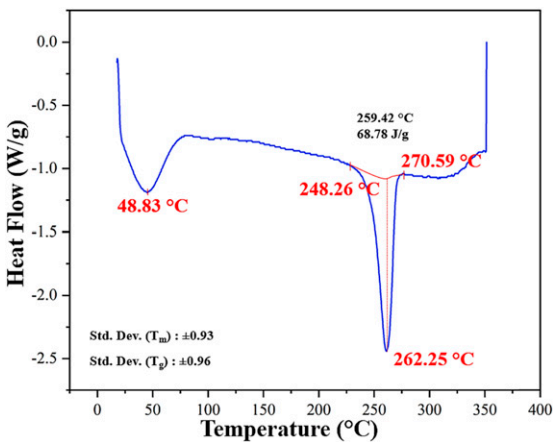


Figure 4. DSC curve of the PA66 veils.

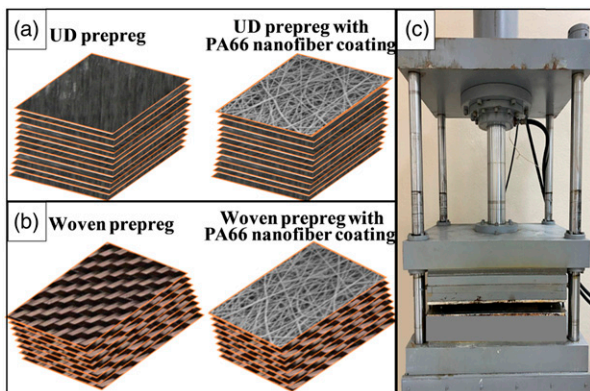


Figure 5. Illustration of composite laminate fabrication. a) 12 layers of unidirectional prepregs at [45/0/45/90/-45/0]s and b) 8 layers of woven prepregs at [45/0/45/0]s with and without electrospun PA66 nanofiber coating. c) The hot press setup used.

experiment and the average values are reported in the manuscript. In addition to the reference samples, a total of 200 samples were tested for the composite joints prepared with two different adhesive layers and three different concentrations of PA66. The dimensions of the test specimens are 180 mm long and 25 mm wide, while the area of overlap area is $25 \times 25 \text{ mm}^2$; as described in Figure 8(c).

Results and discussion

The effects of variation in PA66 solution ratio on the morphology of the resulted nanofiber coatings were studied first. Figure 9 presents the SEM images of PA66 nanofibers produced with the solutions with 10%, 12%, 14%, and 18% of PA66 weight ratios. The nanofiber density increased with increasing PA66%. However, bead formations and clustering were also observed. SEM images show that the fibers produced with 10% wt PA66 solution had a more homogeneous fiber structure than those made at other ratios. Hence, optimum nanofiber morphology with a continuous and uniform network without fiber beads was observed at 10% PA66 solutions. With the corresponding electrospinning operating parameters, an average fiber diameter of $\sim 36 \text{ nm}$ was obtained.

Next, different deposition periods yielding different nanofiber coating thicknesses were studied. Specifically, 3, 7, and 10 min electrospinning were performed, and the resulting fiber coating by measuring their area weight densities was characterized. The nanofibers were carefully stripped from the prepreg surface, cut into specific size small pieces, and weighted with a precision scale. The average PA66 nanofiber area weight density for 3, 7, and 10 min of deposition were measured approximately as 0.525 g/m^2 , 1.205 g/m^2 and 1.782 g/m^2 , respectively. In the

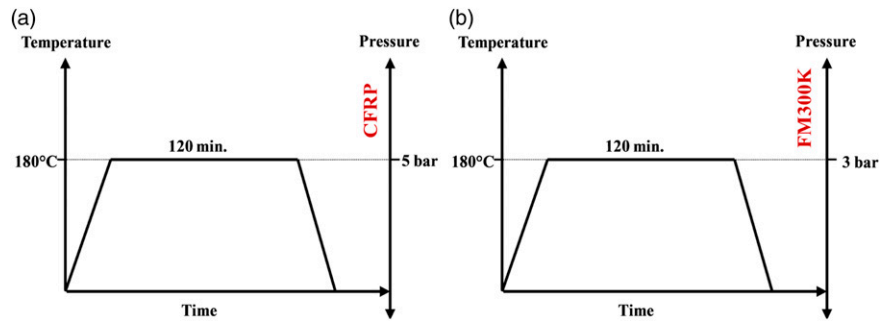


Figure 6. Manufacturing procedure for the hot press curing of a) UD/woven prepregs (CFRP) and b) joint using film adhesive (FM300 K).

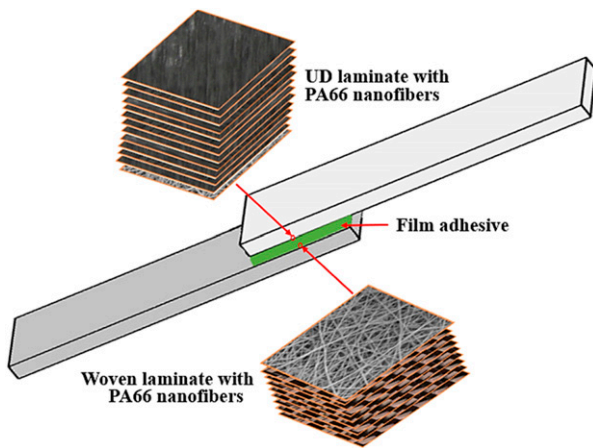


Figure 7. The adhesive joining of UD and woven CFRP fabrics with the electrospun PA66 nanofibers coated at both of the joint interfaces.

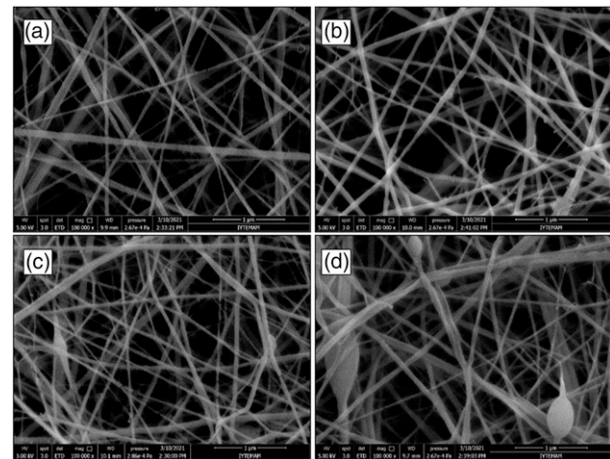


Figure 9. SEM images of electrospun PA66 nanofiber coatings at PA 66 by weight solution ratios of a) 10%, b) 12%, c) 14%, d) 18%.

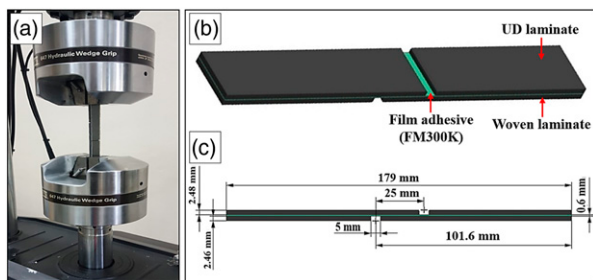


Figure 8. a) Experimental setup for the single-lap joint shear test. b) Illustration of the specimen of adhesively joint UD and woven CFRP parts. c) Dimensions of the lap shear test coupon.

studied deposition time range, the weight gain due to nanofiber coatings observed as less than 2%, which is negligible.

Adhesively joined UD and woven CFRP laminates fabricated with incorporation of electrospun PA66 nanofiber coatings at their interfaces were mechanically tested. At

least five samples were tested for each type of the experiment to calculate the average values. In addition to the reference samples, we tested a total of 200 composite joint samples prepared with using different number of adhesive layers and electrospun PA66 application. A representative set of load versus displacement results for uncoated reference and 10%wt PA66 coated surfaces joined using three layers of adhesive are given in Figure 10. Results obtained from five different sample show high repeatability of the measurements with a very low standard deviation.

The load versus displacement curves of reference, 10% wt-PA66, 12% wt-PA66% and 14% wt-PA66 samples with two and three layers of FM300 K adhesive obtained during single lap shear test are shown in Figure 11. Both the reference samples and the PA66 nanofiber incorporated samples exhibit a linear elastic behavior at the initial stage. Test specimens exhibited a non-linear elastic behavior at further stages of the loadings. It was found that samples prepared with three layers of film adhesive showed a higher performance, as compared to those with two layers of film adhesive.

The average bonding strength values measured based on single-lap shear tests are given in Figure 11 for specimens using different PA66 solutions and adhesive thicknesses. The nanofibers produced with 10, 12, and 14 wt.% of PA66 solutions were interspersed for a 10 min

electrospinning time. It was observed that two and three plies of adhesive application keep the thickness increase minimum. The result of adhesive joints without electrospun nanofiber coating as a reference is presented as well Figure 12.

The shear strengths of the reference composites prepared with two- and 3-layer adhesive were measured as 8.50 and 8.91 MPa, respectively. Compared to the reference sample, a substantial increase in shear strength was observed; the shear strength of the PA66 nanofiber layers incorporated samples using three layers of film adhesive showed about 38% increase in bond strength. Our measurements showed that the highest shear strength values are obtained at 10% PA66 solution with three layers of FM300 K adhesive use. The nanofibers produced from 10%wt PA66 polymer solution resulted with a greater improvement in mechanical performance as compared to those prepared with other solution concentrations. This is due to the uniform fiber diameter distribution with bead-free nanofiber structures as we observed from SEM images.

Literature describes that the joint strength as a function of the adhesive thickness varies depending on the adhesive type, joining technique and surface modification approach.^{5,35-38} While the bending moment is expected to increase by the increasing adhesive thickness, using paste and liquid type adhesives were observed to yield in joint strength reduction for increasing adhesive thickness. On the other hand, the recent film adhesive applications showed improved joint strength with increased adhesive thickness^{5,39-43}. These studies investigated comparable behavior and showed that film adhesives with even thickness distribution creates an advantage. The FM300 K aerospace-grade film adhesive yielded to improved joint strength with increased adhesive thickness, similar to the literature.⁵

As the final step, fractured surface of adhesive joints of composites were investigated. The images of the joint regions after the lap shear tests are given in Figure 13. Specifically, the fracture surfaces of specimens produced

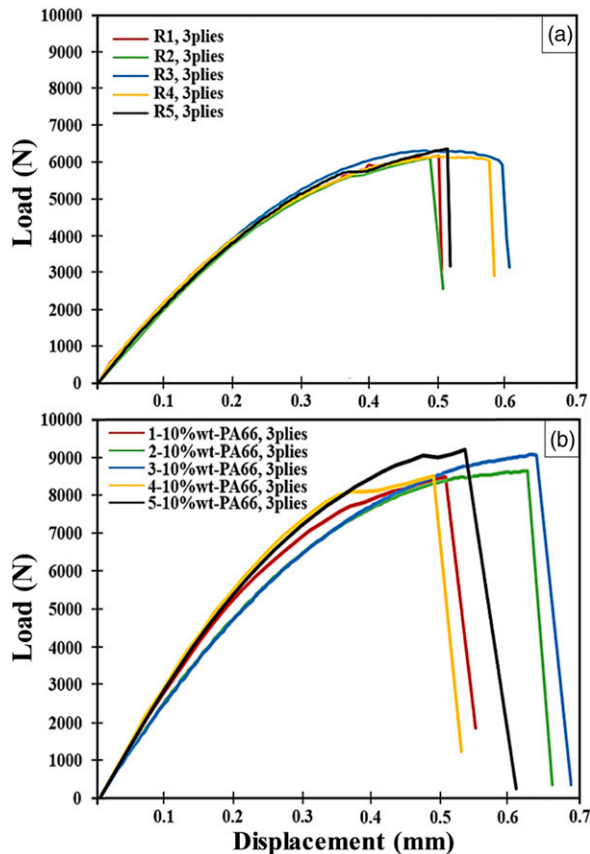


Figure 10. The load versus displacement curves of single lap shear tests of five different samples of a) uncoated reference, and b) 10% wt-PA66-3 coated surfaces joined using three FM300 K plies.

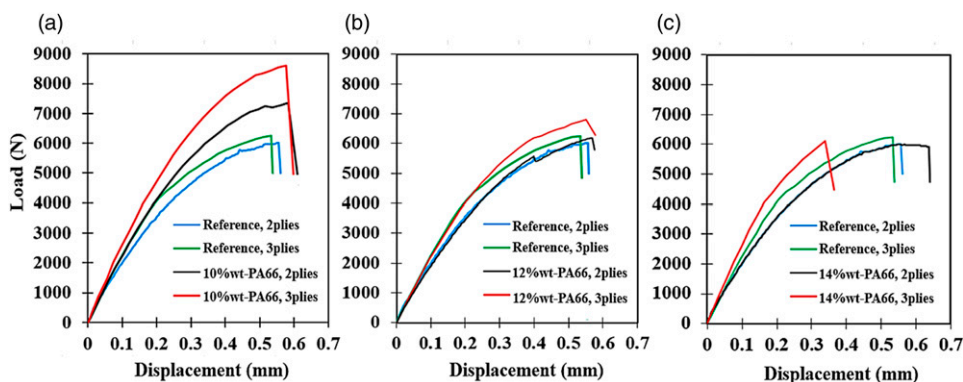


Figure 11. The load versus displacement curves of reference, a) 10% wt-PA66, b) 12% wt-PA66 and c) 14% wt-PA66 samples with two and three plies of FM300 K adhesive obtained during single lap shear test.

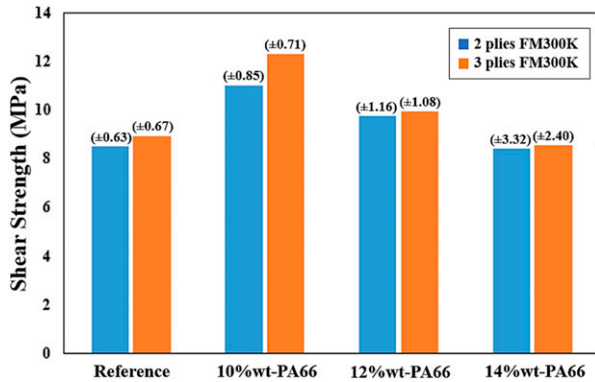


Figure 12. The shear strength values of adhesively bonded UD and woven CFRP parts with/without PA66 electrospun fiber layers with various electrospinning solutions and amounts.

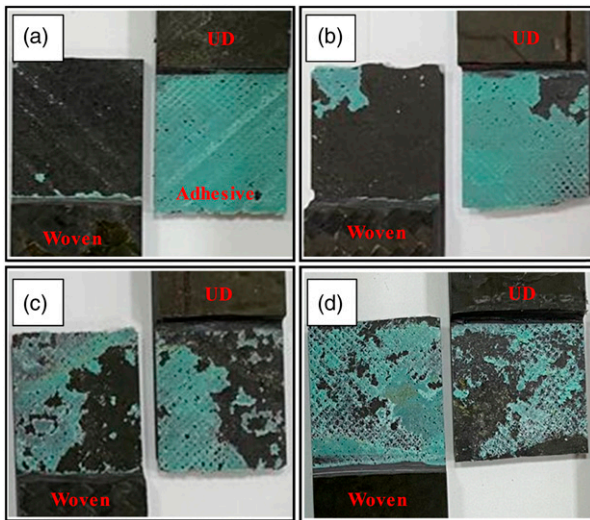


Figure 13. The fractured surfaces after single lap shear test. Woven and UD parts joined with a) no-nanofiber coating and 2-ply of FM300 K, b) no-nanofiber coating and 3-ply of FM300 K, c) 10wt% PA66 nanofiber coating and 2-ply of FM300 K, and d) 10wt% PA66 nanofiber coating and 3-ply of FM300 K.

with and without electrospun nanofiber coating with two- and 3-ply of adhesive applications were compared. In Figure 13, woven specimens are on the left while the UD parts are given on the right-hand side. The light-colored (green) material on the joining interfaces is the adhesive used. It can be seen from Figures 13(a) and (b) that adhesive material mostly remains on only one of the joining surfaces after the breakage for the samples without nanofiber coating. This indicates interfacial debonding at composite/adhesive surfaces to a premature adhesive failure. On the other hand, the adhesive material can be observed on both surfaces when nanofibers are added to the interface. The cohesive failure of the adhesive is obvious indicating better interfacial bonding between composite/adhesive surfaces. In other words, it was revealed that the PA66 nanofibers incorporated samples adhere to the adhesive better than the bare surface. As expected from the increased shear strengths measured by lab-shear tests, the samples joined using three layers of film adhesive showed better adhesion performance as compared to the samples combined with two layers.

The fractured surface SEM images of joined composites are given in Figure 14. Large adhesive flakes are visible on Figure 14(a) over the CFRP surface without the nanofiber coating. Instead, adhesive is well penetrated into the nanofiber network developed as the electrospun PA66 added onto interface (Figures 14(b) and (c)). A better cohesion of film adhesive develops with increasing the number of adhesive layers used. Results showed that coating PA66 nanofibers on the prepreps enhanced bonding between adhesive and the composite surfaces for joining. The adhesive used in the present study is a high performance type. So, it is not to expect a cohesive failure with the adhesive layers. The nano fibers were incorporated to the composite surfaces to obtain relatively higher interfacial adhesion between composite surfaces and the adhesive layers. A relatively higher bonding strength values were obtained with the joints containing nanolayers at the composite surfaces as compared to those with reference samples with no nanofiber coatings. Reference samples exhibited an adhesive failure on single side of the

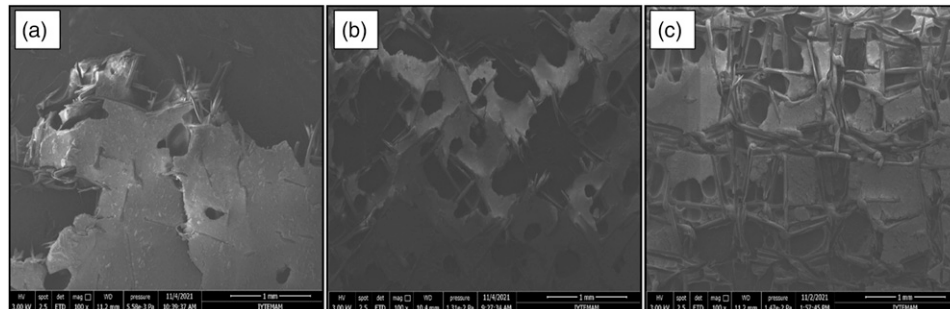


Figure 14. SEM surface images of adhesive joints after breakage. a) no-nanofiber coating and 3-ply of FM300 K, b) 10wt% PA66 nanofiber coating and 2-ply of FM300 K, and c) 10wt% PA66 nanofiber coating and 3-ply of FM300 K.

interface. However, the failure characteristics are different as debonding mechanism exist in micro level between nanofiber coated surface layers and adhesive layers as compared to surfaces without nanolayers. In summary, the nano fibers layers on the surface assign the failure mode and provide an improved joint strength.

Conclusions

Use of composite materials have been increasing in various industrial applications, from aircraft parts to bottle caps. The adhesive joining techniques appeared as an excellent alternative to traditional mechanical fastening posing so many cons. For the first time in literature, the electrospun nanofibers coating of the adhesive bonding interfaces to enhance the bonding strength were performed at a low adhesive thickness and weight gain. The study specifically focused on the electrospinning of PA66 due to its numerous advantages, such as being inexpensive, dissolving quickly in a wide variety of solvents, having negligible post-coating thickness increase, and having better mechanical properties compared to other polymers. Furthermore, the study focused on secondary bonding of UD and woven CFRP parts, since it is preferred in most aerospace applications.

The secondary bonding of UD and woven parts by applying nanofiber coating with different PA66 electrospinning solutions, different electrospinning duration, and different adhesive thicknesses were studied. Morphological characterization using SEM images was performed to carefully optimize application parameters to obtain homogeneous and beadless nanofiber production. The single-lap shear tests were performed to demonstrate the effects of PA66 on the adhesion properties. As a result, about 40% increase was observed in the shear strength values by nanofiber application on both joining surfaces. When the fractured surfaces through SEM analysis were studied, it was observed that nanofiber coated joints develop coherent failure while the bare surfaces yield adhesive breakage. The PA66 nanofibers provide better coupling between the adhesive and the composite surface and hence higher bonding strength by increasing the surface area and roughness. As a result, electrospun nanofibers turned premature adhesive failure into cohesive adhesion failure and enhanced the adhesion performance composite joints substantially.

Acknowledgements

The authors acknowledge the Scientific and Technological Research Council of Turkey (TUBITAK) for financial support and Turkish Aerospace Industries Inc. (TUSAS) of Turkey for providing carbon prepregs and adhesive materials. Also, the authors

acknowledge IZTECH Center for Materials Research (MAM) for providing testing services in this study.

Declaration of conflicting interests

The author(s) declared no potential conflicts of interest with respect to the research, authorship, and/or publication of this article.

Funding

The author(s) disclosed receipt of the following financial support for the research, authorship, and/or publication of this article: This work was supported by the Scientific and Technological Research Council of Turkey (TUBITAK) under Grant Number 218M701.

ORCID iDs

Murat Barisik  <https://orcid.org/0000-0002-2413-1991>
Metin Tanoglu  <https://orcid.org/0000-0001-9770-1302>
Engin Aktas  <https://orcid.org/0000-0002-5706-2101>

References

1. Brito CBG, De Cássia Mendonça Sales Contini R, Gouvêa RF, De Oliveira AS, Arbelo MA and Donadon MV. Mode I interlaminar fracture toughness analysis of Co-bonded and secondary bonded carbon fiber reinforced composites joints. *Mater Res* 2017; 20: 873–882, DOI: [10.1590/1980-5373-mr-2016-0805](https://doi.org/10.1590/1980-5373-mr-2016-0805).
2. Encinas N, Oakley BR, Belcher MA, Blohowiak KY, Dillingham RG, Abenojar J and Martínez MA. Surface modification of aircraft used composites for adhesive bonding. *Int J Adhes Adhesives* 2014; 50: 157–163, DOI: [10.1016/j.ijadhadh.2014.01.004](https://doi.org/10.1016/j.ijadhadh.2014.01.004).
3. Noor AK, Venneri SL, Paul DB and Hopkins MA. Structures technology for future aerospace systems. *Comput Structures* 2000; 74(5): 507–519, DOI: [10.1016/S0045-7949\(99\)00067-X](https://doi.org/10.1016/S0045-7949(99)00067-X).
4. Uz YC. *Development and characterization of innovative fiber reinforced prepregs and their composites containing functional fillers (issue july)*, 2021.
5. Song MG, Kweon JH, Choi JH, Byun JH, Song MH, Shin SJ and Lee TJ. Effect of manufacturing methods on the shear strength of composite single-lap bonded joints. *Compos Structures* 2010; 92(9): 2194–2202, DOI: [10.1016/j.compstruct.2009.08.041](https://doi.org/10.1016/j.compstruct.2009.08.041).
6. Moretti L, Olivier P, Castanié B and Bernhart G. Experimental study and in-situ FBG monitoring of process-induced strains during autoclave co-curing, co-bonding and secondary bonding of composite laminates. *Composites A: Appl Sci Manufacturing* 2021; 142: 106224, DOI: [10.1016/j.compositesa.2020.106224](https://doi.org/10.1016/j.compositesa.2020.106224).
7. Fleuret C, Andreani AS, Lainé É, Grandidier JC, L'Héritier S and Gorge AL. Complex wing spar design in carbon fiber

- reinforced composite for a light aerobatic aircraft. *Mech Industry* 2016; 17(6): 614, DOI: [10.1051/meca/2016032](https://doi.org/10.1051/meca/2016032).
8. Hélénon F, Wisnom MR, Hallett SR and Trask RS. Numerical investigation into failure of laminated composite T-piece specimens under tensile loading. *Composites Part A: Appl Sci Manufacturing* 2012; 43(7): 1017–1027, DOI: [10.1016/j.compositesa.2012.02.010](https://doi.org/10.1016/j.compositesa.2012.02.010).
 9. Budhe S, Banea MD, de Barros S and da Silva LFM. An updated review of adhesively bonded joints in composite materials. *Int J Adhes Adhesives* 2017; 72(October): 30–42, DOI: [10.1016/j.ijadhadh.2016.10.010](https://doi.org/10.1016/j.ijadhadh.2016.10.010).
 10. Li X, Tao R, Yudhanto A and Lubineau G. How the spatial correlation in adhesion properties influences the performance of secondary bonding of laminated composites. *Int J Sol Structures* 2020; 196–197: 41–52, DOI: [10.1016/j.ijsolstr.2020.04.012](https://doi.org/10.1016/j.ijsolstr.2020.04.012).
 11. Mohan J, Ivanković A and Murphy N. Mode I fracture toughness of co-cured and secondary bonded composite joints. *Int J Adhes Adhesives* 2014; 51: 13–22, DOI: [10.1016/j.ijadhadh.2014.02.008](https://doi.org/10.1016/j.ijadhadh.2014.02.008).
 12. Mohan J, Ivanković A and Murphy N. Mixed-mode fracture toughness of co-cured and secondary bonded composite joints. *Eng Fracture Mech* 2015; 134: 148–167, DOI: [10.1016/j.engfracmech.2014.12.005](https://doi.org/10.1016/j.engfracmech.2014.12.005).
 13. Mazumdar SK and Mallick PK. Static and fatigue behavior of adhesive joints in SMC-SMC composites. *Polym Composites* 1998; 19(2): 139–146, DOI: [10.1002/pc.10084](https://doi.org/10.1002/pc.10084).
 14. Beylergil B, Tanoğlu M and Aktaş E. Enhancement of interlaminar fracture toughness of carbon fiber–epoxy composites using polyamide-6, 6 electrospun nanofibers. *J Appl Polym Sci* 2017; 134(35): 1–12, DOI: [10.1002/app.45244](https://doi.org/10.1002/app.45244).
 15. Kim C, Park SH, Lee WJ and Yang KS. Characteristics of supercapacitor electrodes of PBI-based carbon nanofiber web prepared by electrospinning. *Electrochimica Acta* 2004; 50(2–3): 877–881, DOI: [10.1016/j.electacta.2004.02.071](https://doi.org/10.1016/j.electacta.2004.02.071).
 16. Lam HL. *Electrospinning of single wall carbon nanotube reinforced aligned fibrils and yarns*. A Thesis Submitted to the Faculty of Drexel University, 2004, p. 246. 2004(October) <http://onlinelibrary.wiley.com/doi/10.1002/cbdv.200490137/abstract>
 17. Lyons J, Li C and Ko F. Melt-electrospinning part I: Processing parameters and geometric properties. *Polymer* 2004; 45(22): 7597–7603, DOI: [10.1016/j.polymer.2004.08.071](https://doi.org/10.1016/j.polymer.2004.08.071).
 18. Mohan A. *Formation and characterization of electrospun nonwoven webs*. Textile Management and Technology, 2002, <https://www.mendeley.com/viewer/?fileId=789cf426-0a97-dd89-4e13-fa027cfe584a&documentId=c2902bde-2e32-39df-80cd-8f3b76838cea>
 19. Jentzsch E, Gül Ö and Öznergiz E. A comprehensive electric field analysis of a multifunctional electrospinning platform. *J Electrostatics* 2013; 71(3): 294–298, DOI: [10.1016/j.elstat.2012.12.007](https://doi.org/10.1016/j.elstat.2012.12.007).
 20. Niu H, Wang X and Lin T. Needleless electrospinning: Influences of fibre generator geometry. *J Textile Inst* 2012; 103(7): 787–794, DOI: [10.1080/00405000.2011.608498](https://doi.org/10.1080/00405000.2011.608498).
 21. Aljarrah MT and Abdelal NR. Improvement of the mode I interlaminar fracture toughness of carbon fiber composite reinforced with electrospun nylon nanofiber. *Composites B: Eng* 2019; 165: 379–385, DOI: [10.1016/j.compositesb.2019.01.065](https://doi.org/10.1016/j.compositesb.2019.01.065).
 22. Beckermann GW and Pickering KL. Mode I and Mode II interlaminar fracture toughness of composite laminates interleaved with electrospun nanofibre veils. *Composites Part A: Appl Sci Manufacturing* 2015; 72: 11–21, DOI: [10.1016/j.compositesa.2015.01.028](https://doi.org/10.1016/j.compositesa.2015.01.028).
 23. Daelemans L, van der Heijden S, De Baere I, Rahier H, Van Paeppegem W and De Clerck K. Nanofibre bridging as a toughening mechanism in carbon/epoxy composite laminates interleaved with electrospun polyamide nanofibrous veils. *Composites Sci Technology* 2015; 117: 244–256, DOI: [10.1016/j.compscitech.2015.06.021](https://doi.org/10.1016/j.compscitech.2015.06.021).
 24. Matulevicius J, Kliucininkas L, Martuzevicius D, Krugly E, Tichonovas M and Baltrusaitis J. Design and characterization of electrospun polyamide nanofiber media for air filtration applications. *J Nanomater* 2014; 2014: 1–13, DOI: [10.1155/2014/859656](https://doi.org/10.1155/2014/859656).
 25. Saz-orozco D, Ray D and Stanley WF. *Effect of thermoplastic veils on interlaminar fracture toughness of a glass fiber/vinyl ester composite*, 2015, DOI: [10.1002/pc.23840](https://doi.org/10.1002/pc.23840).
 26. Arboleda-Clemente L, Ares-Pernas A, García X, Dopico S and Abad MJ. Influence of polyamide ratio on the CNT dispersion in polyamide 66/6 blends by dilution of PA66 or PA6-MWCNT masterbatches. *Synth Met* 2016; 221: 134–141, DOI: [10.1016/j.synthmet.2016.07.030](https://doi.org/10.1016/j.synthmet.2016.07.030).
 27. Lee CJ, Salehiyan R, Ham DS, Cho SK, Lee SJ, Kim KJ, Yoo Y, Hyun K, Lee JH and Choi WJ. Influence of carbon nanotubes localization and transfer on electrical conductivity in PA66/(PS/PPE)/CNTs nanocomposites. *Polymer* 2016; 84: 198–208, DOI: [10.1016/j.polymer.2015.12.055](https://doi.org/10.1016/j.polymer.2015.12.055).
 28. Lee M, Son K, Kim J, Kim D, Min BH and Kim JH. Effect of PA6T on morphology and electrical conductivity in PA66/PA6T/PPE/multiwalled carbon nanotube nanocomposites. *Composites Sci Technology* 2018; 164(February): 260–266, DOI: [10.1016/j.compscitech.2018.05.049](https://doi.org/10.1016/j.compscitech.2018.05.049).
 29. Umesh GL, Krishna Prasad NJ, Rudresh BM and Devegowda M. Influence of nano graphene on mechanical behavior of PA66/PA6 blend based hybrid nano composites: Effect of micro fillers. *Mater Today Proc* 2020; 20(xxxx): 228–235, DOI: [10.1016/j.matpr.2019.12.222](https://doi.org/10.1016/j.matpr.2019.12.222).
 30. Kang DH and Kang HW. Surface energy characteristics of zeolite embedded PVDF nanofiber films with electrospinning process. *Appl Surf Sci* 2016; 387: 82–88, DOI: [10.1016/j.apsusc.2016.06.096](https://doi.org/10.1016/j.apsusc.2016.06.096).
 31. Beigmoradi R, Samimi A and Mohebbi-Kalhari D. Fabrication of polymeric nanofibrous mats with controllable structure and enhanced wetting behavior using one-step

- electrospinning. *Polymer* 2018; 143: 271–280, DOI: [10.1016/j.polymer.2018.04.025](https://doi.org/10.1016/j.polymer.2018.04.025).
32. Stachewicz U and Barber AH. Enhanced wetting behavior at electrospun polyamide nanofiber surfaces. *Langmuir* 2011; 27(6): 3024–3029, DOI: [10.1021/la1046645](https://doi.org/10.1021/la1046645).
 33. Sanatgar RH, Borhani S, Ravandi SAH and Gharehaghaji AA. The influence of solvent type and polymer concentration on the physical properties of solid state polymerized PA66 nanofiber yarn. *J Appl Polym Sci* 2012; 126(3): 1112–1120, DOI: [10.1002/app.36871](https://doi.org/10.1002/app.36871).
 34. Mohan A, Lyons J, Li C, Ko F, Liker JK, Huang ZM, Zhang YZ, Kotaki M and Ramakrishna S. A review on polymer nanofibers by electrospinning and their applications in nanocomposites. *Composites Sci Technology* 2004; 63(15): 2223–2253, DOI: [10.1016/S0266-3538\(03\)00178-7](https://doi.org/10.1016/S0266-3538(03)00178-7).
 35. Guo L, Liu J, Xia H, Li X, Zhang X and Yang H. Effects of surface treatment and adhesive thickness on the shear strength of precision bonded joints. *Polym Test* 2021; 94: 107063, DOI: [10.1016/j.polymertesting.2021.107063](https://doi.org/10.1016/j.polymertesting.2021.107063).
 36. Ji G, Ouyang Z, Li G, Ibekwe S and Pang SS. Effects of adhesive thickness on global and local mode-I interfacial fracture of bonded joints. *Int J Sol Structures* 2010; 47(18–19): 2445–2458, DOI: [10.1016/j.ijsolstr.2010.05.006](https://doi.org/10.1016/j.ijsolstr.2010.05.006).
 37. Liao L, Huang C and Sawa T. Effect of adhesive thickness, adhesive type and scarf angle on the mechanical properties of scarf adhesive joints. *Int J Sol Structures* 2013; 50(25–26): 4333–4340, DOI: [10.1016/j.ijsolstr.2013.09.005](https://doi.org/10.1016/j.ijsolstr.2013.09.005).
 38. Naito K, Onta M and Kogo Y. The effect of adhesive thickness on tensile and shear strength of polyimide adhesive. *Int J Adhes Adhesives* 2012; 36: 77–85, DOI: [10.1016/j.ijadhadh.2012.03.007](https://doi.org/10.1016/j.ijadhadh.2012.03.007).
 39. Castagnetti D, Spaggiari A and Dragoni E. Robust shape optimization of tubular butt joints for characterizing thin adhesive layers under uniform normal and shear stresses. *J Adhes Sci Technology* 2010; 24(11–12): 1959–1976, DOI: [10.1163/016942410X507687](https://doi.org/10.1163/016942410X507687).
 40. Ke L, Li C, Luo N, He J, Jiao Y and Liu Y. Enhanced comprehensive performance of bonding interface between CFRP and steel by a novel film adhesive Composite Structures. *Compos Structures* 2019; 229(June): 111393, DOI: [10.1016/j.compstruct.2019.111393](https://doi.org/10.1016/j.compstruct.2019.111393).
 41. Matthews FL and Tester TT. The influence of stacking sequence on the strength of bonded CFRP single lap joints. *Int J Adhes Adhesives* 1985; 5(1): 13–18, DOI: [10.1016/0143-7496\(85\)90040-5](https://doi.org/10.1016/0143-7496(85)90040-5).
 42. Peng X, Liu S, Huang Y and Sang L. Investigation of joining of continuous glass fibre reinforced polypropylene laminates via fusion bonding and hotmelt adhesive film. *Int J Adhes Adhesives* 2020; 100: 102615, DOI: [10.1016/j.ijadhadh.2020.102615](https://doi.org/10.1016/j.ijadhadh.2020.102615).
 43. Wang CH and Chalkley P. Plastic yielding of a film adhesive under multiaxial stresses. *Int J Adhes Adhesives* 2000; 20(2): 155–164, DOI: [10.1016/S0143-7496\(99\)00033-0](https://doi.org/10.1016/S0143-7496(99)00033-0).